Real-time Monitoring of Temperature Field Distribution of Three-element LiB Lithium Battery Using FBG Arrays

Feixia Huang, Hong Yang, Bin Liu, Juan Liu, Yingying Hu, Yue Fu, Wenbo Xiao, Xing-Dao He, Qiang Wu

***Abstract*—Temperature has a significant impact on the health and safety lifespan of lithium-ion batteries. In this paper, we propose a monitoring network consisting of 32 fiber Bragg grating (FBG) sensors for real-time monitoring of the battery surface temperature. The temperature points measured by FBG sensors are used to construct the temperature distribution of the entire battery surface, enabling monitoring of the hotspots during the battery charging and discharging process. The battery was subjected to 0.5C, 1C, and 1.5C rate charging and discharging tests during the experiment. The results show that the battery surface temperature decreases gradually from the position close to the positive and negative electrode tabs to the position away from the positive and negative electrode tabs, and the temperature near the negative electrode tabs is the highest. The highest temperature rises during the first charging and discharging test at 0.5C, 1C, and 1.5C rates are 14.9 °C, 30.4 °C, and 38.4 °C, respectively. Additionally, the dynamic graph of the battery surface temperature change is constructed by the monitoring network composed of FBG sensors, which can reflect the real-time and intuitive distribution of the battery surface temperature during charging and discharging. Therefore, the proposed temperature monitoring network can accurately monitor the time and space of hotspots on the battery surface, improving the safety of battery operation.**

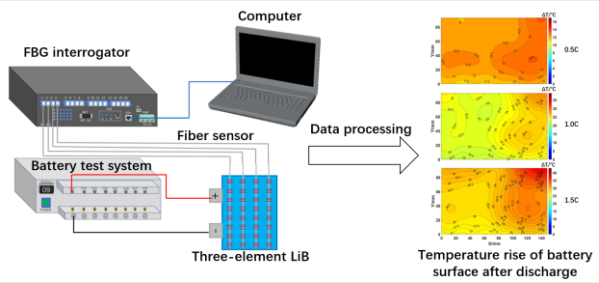

***Index Terms*—Three-element LiB Lithium Battery; Fiber Bragg Grating; Temperature Monitoring.**

I. Introduction

LITHIUM-ION batteries (LiBs) are widely used in mobile devices, electric vehicles, household appliances, and the industrial sector due to their high energy density, long lifespan, and low self-discharge rate [1-3]. However, the safety of batteries is a major constraint on the development of LiB. The working temperature of LiB is considered to be the most important factor affecting battery safety [4-9]. Both high and low temperatures can affect the performance and lifespan of LiB, with high temperature having the greatest impact on battery health and lifespan. High temperature can accelerate the chemical reactions and corrosion inside LiB, leading to a decrease in battery capacity and lifespan. At extremely high temperature, LiB may experience thermal runaway, causing safety issues such as fire and explosion. Battery thermal management can monitor the working status of batteries in real-time, keeping them operating within an appropriate temperature range to maintain optimal performance [10]. Among them, temperature monitoring is the most important task in battery thermal management [11-13]. Currently, there are many methods used to monitor the battery temperature during operation, with the most commonly used method being a Positive Temperature Coefficient (PTC) thermistor. The PTC thermistor is a material whose resistance increases as the temperature rises. Therefore, installing a PTC thermistor inside a LiB can monitor its internal temperature. In addition, the PTC thermistor can also be used to control the charging rate and charging cut-off voltage of LiB to prevent overheating. Another commonly used method is a thermocouple. Due to its high sensitivity and fast response, the thermocouple is widely used for temperature monitoring on the surface of batteries. However, for large battery modules, the thermocouple can only measure a single point, making it extremely susceptible to short circuits for hundreds or thousands of individual battery cells. Therefore, it is difficult to use in large battery modules with an increasing number of individual battery cells [14-15]. Infrared sensors are also used for battery temperature measurement due to their operational convenience. Compared with measurement methods of contact temperature, non-contact temperature measurement can be achieved, avoiding the shortcomings of thermocouples, which are prone to short circuits. However, due to the scattering and reflection of infrared rays, their accuracy is greatly affected by environmental factors and can only roughly measure the battery surface temperature [16]. FBG sensors have been widely used in the sensing field due to their advantages of small size, non-conductivity, electromagnetic interference resistance,

This work was supported in part by the National Natural Science Foundation of China (NSFC) under Grants 62365013, 62175097, and 62065013) and in part by the 03 Special Project and 5G Project of Jiangxi Province under Grant 20232ABC03A05. (*Corresponding author: Bin Liu, Qiang Wu*)

Feixia Huang, Hong Yang, Bin Liu, Juan Liu, Yingying Hu, Yue Fu, Wenbo Xiao, Xing-Dao He, Qiang Wu are with the Key Laboratory of Opto-Electronic Information Science and Technology of Jiangxi Province, Nanchang Hangkong University, Nanchang 330063, China. (e-mail: liubin_d@126.com; qiang.wu@northumbria.ac.uk)

Qiang Wu is with the Faculty of Engineering and Environment, Northumbria University, Newcastle Upon Tyne, NE1 8ST, United Kingdom.

and multi-point measurement, such as human-computer interaction, healthcare, and health detection [17,18]. Accurate real-time monitoring can also be carried out for highly integrated large battery modules [19,20].

There is much literature on using FBG sensors to monitor battery temperature. Fortier et al. implanted FBG sensors into coin cells to monitor the cell temperatures at different charge/discharge rates [21]. Fleing et al. directly inserted FBG sensors into cylindrical LiB to achieve precise measurement of internal battery temperature [22]. Since there are gaps in the middle of cylindrical batteries, the FBG sensor inserted inside will not be affected by the battery strain and can monitor the internal temperature of the battery effectively [23,24]. Vitorino Biazi et al. used the filter-based virtual sensor to estimate the charging state of the battery and detect internal temperature [25]. However, for square LiB, which adopts a winding packaging method inside, there are no gaps, and this internal measurement method cannot be used to detect such square battery temperature. In addition to measuring the internal battery temperature, there are also many examples of measuring the battery surface temperature. Lucca C et al. used birefringent PANDA optical fibers to detect the surface temperature and strain of 18650 LiB [26]. Similarly, Lucca Matuck et al. used polarization-maintaining FBG to detect the surface temperature and strain of LiB [27]. Juu Peng et al. used an FBG sensor wrapped around a metal ring to measure the temperature of the positive and negative terminals of the battery during operation for thermal management. However, due to the resistance of the positive and negative terminals, there will be some heat generated during charging and discharging, so measuring only the temperature of the terminals is not enough to reflect the temperature status of the entire battery [28]. Nascimento et al. used three cascaded FBG sensors arranged on the surface of a mobile phone battery to monitor the temperature changes during charging and discharging [29,30]. S. Ferreira et al. monitored the temperature of the four sides of a battery pack using 12 FBG sensors to identify the hotspots and improve battery thermal management [31]. The result shows significant temperature differences between the FBG sensors, indicating an uneven temperature distribution (TD) on the battery surface during charging and discharging cycles. Due to limitations in the number and placement of sensors, the temperature measurement of the battery surface using FBG sensors can only monitor specific points, leading to uncertainties in identifying hotspots and reflecting the overall TD of the battery surface.

In this paper, we construct a temperature sensing network on the surface of a LiB using 32 FBG sensors. By appropriately increasing the number of sensors, we aim to improve the coverage of the temperature sensing network on the battery surface. Through the measurements of the 32 temperature points, we construct a temperature field on the battery surface that dynamically reflects the changes in battery surface temperature, enabling accurate identification of the temporal and spatial distribution of hotspots on the battery surface. In future research, an integrated parameter thermal model of the battery will be constructed to predict the temperature distribution inside the battery [32-34].

At charging and discharging rates of 0.5C, 1C, and 1.5C, the hotspots are mainly located near the positive and negative electrode taps of the battery, with the most significant hotspot being near the negative electrode taps. And the highest temperatures on the battery surface increase by 14.9 °C, 30.4 °C, and 38.4 °C during the first charging and discharging tests at 0.5C, 1C, and 1.5C rates, respectively. Our results show that the proposed FBG temperature sensing network has an accuracy of ±0.2 °C and could accurately measure the TD on the battery surface, providing valuable data for battery thermal management and a better understanding of the working status of the battery during charging and discharging.

II. Experimental Procedure and Test

A. Layout Design of FBG Sensing Network

The experiment used single-mode optical fiber model BI1015B-B manufactured by YOFC Optical Fiber and Cable Co., Ltd, and the FBG arrays were prepared using traditional excimer laser exposure and phase mask fabrication method [35]. According to the geometric dimensions of the battery, we used four identical optical fibers (each optical fiber has 8 FBG sensors, with a length and spacing of 5 mm and 12 mm, respectively, and each central wavelength of FBG is shown in Table 1) arranged at four positions on the battery surface. One end of the optical fiber was attached to the battery using epoxy resin adhesive with model E-120HP, and the other end was connected to the battery through a PVC tube, allowing the optical fiber to expand freely.

TABLE I
CENTER WAVELENGTHS OF THE FBGS

Optical fiber	FBG1 (nm)	FBG2 (nm)	FBG3 (nm)	FBG4 (nm)
1	1529.08	1531.67	1533.77	1535.90
2	1529.20	1532.14	1533.84	1536.66
3	1529.97	1531.98	1534.02	1535.98
4	1529.07	1531.65	1533.63	1536.25
Optical fiber	FBG5 (nm)	FBG6 (nm)	FBG7 (nm)	FBG8 (nm)
1	1538.26	1540.17	1542.67	1544.38
2	1538.64	1540.69	1542.49	1544.62
3	1537.94	1539.97	1541.96	1544.02
4	1538.07	1540.33	1542.50	1544.53

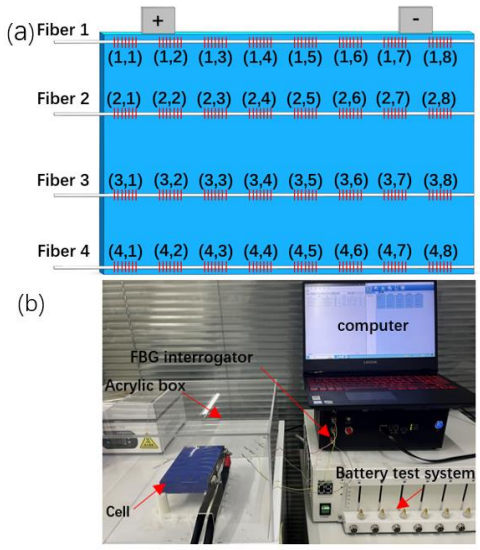

Fig. 1. Battery testing system: (a) Arrangement of FBG sensors on the battery surface; (b) Battery charge-discharge temperature detection system.

As shown in Fig. 1(a), a total of 32 FBG sensors form a 4×8 matrix sensing network to monitor the battery surface temperature. The position of each FBG sensor relative to the battery is represented in matrix (i, j) format, where i=1,2,3,4 represents the number of each optical fiber, and j=1,2,3,4,5,6,7,8 represents the corresponding serial number of the FBG sensor on each optical fiber.

In order to improve the temperature measurement accuracy of the FBG sensor, we calibrated its temperature sensitivity before placing it on the battery surface. An intelligent constant temperature platform (BY-2020, Bangyuan Electronics Co., Ltd., China) was used to calibrate the FBG sensors at increments of 10 °C between 20-60 °C. Figure 2 shows the wavelength shift of each FBG center wavelength on four optical fibers within the calibration temperature range, indicating that the sensitivity of all sensors varies between 9.37-10.33pm/°C.

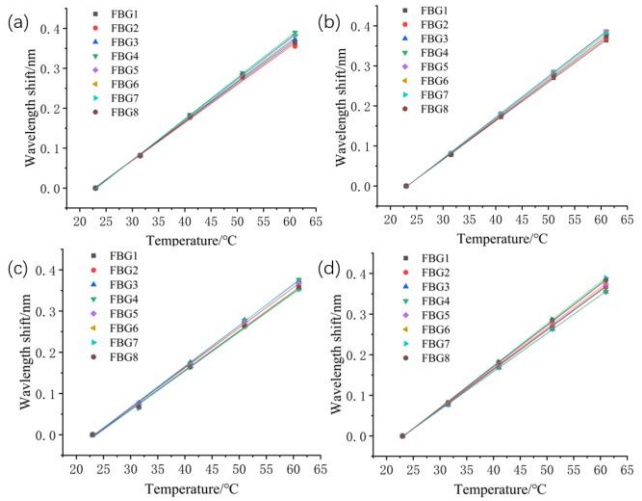

Fig. 2. Sensitivity of the FBG sensors on each optical fiber in the range of 20-60 °C: (a) Optical fiber 1, (b) Optical fiber 2, (c) Optical fiber 3, (d) Optical fiber 4.

B. Battery Test

The ternary lithium battery model ICP27/148/93 was used in this experiment with a nominal voltage of 3.7 V, and a rated capacity of 40 Ah, manufactured by CATL. In the experiment, we used a battery charge-discharge tester (BTS-5100, Shenzhen Bida Testing Technology Co., Ltd., China) to conduct charging and discharging tests at three different rates of 0.5C, 1C, and 1.5C, and performed three complete cycle charging and discharging tests at each rate. To detect the temperature status of the battery surface during charging and discharging, we fully charged and discharged the battery, and the complete charging and discharging cycle test process is shown in Table 2.

The temperature changes on the battery surface were detected by a temperature sensing network consisting of 32 FBG sensors, and the temperature response data of the FBG sensors were synchronously recorded by an optical fiber grating demodulator (TV130, Beijing Tongwei Technology Co., Ltd., China). The entire charging and discharging temperature test was conducted under ambient temperature condition and the battery was placed inside an acrylic box to reduce the influence of the external environment. The battery charging and discharging temperature detection system is shown in Fig. 1(b).

TABLE II
BATTERY CHARGING AND DISCHARGING STEPS

Test procedures	Rate/Voltage	Cut-off Voltage/Current
Constant current discharge	0.5C/1C/1.25C	2.75 V
Rest time	30 min	
Constant current charge	0.5C/1C/1.25C	4.2 V
Constant voltage charge	4.2 V	0.8 A
Rest time	30 min	

III. RESULTS AND DISCUSSION

A. Thermal Behavior of Battery During Standard Charging and Discharging

The voltage, current, and temperature response of FBG sensors in a battery during standard charging and discharging cycles at three different rates are shown in Fig. 3. It can be observed that the temperature response of the FBG sensors is highly consistent with the voltage and current signals in the battery. Taking the first charging and discharging process of a battery at 0.5C as an example, the temperature on the battery surface increases continuously with the decrease in battery voltage during constant current (CC) discharge, and the highest temperature point increases by 14.9 °C when the discharge ends. During the idle period, the battery stops charging and discharging, and the voltage at both ends has a small rebound. At this time, the battery surface temperature has decreased within the range of 6.0 °C to 6.5 °C higher than the initial temperature. Then, the battery enters the charging stage, and during the CC charging process, the battery surface temperature begins to rise again with the increase in voltage until the highest temperature point increases by 14.2 °C when it enters the constant voltage (CV) charging stage. During the CV charging process, as the CC decreases, the battery surface temperature also decreases continuously to 1.5 °C to 2.0 °C higher than the initial temperature.

Through the changes in the temperature response of each FBG sensor in Fig. 3(b-e), it can be found that the temperature change trend of each temperature measurement point on the surface of the battery is consistent. However, there are still significant temperature differences between different temperature points at the same time. The hotspots with higher temperature during battery charging and discharging are mainly distributed near the positive and negative electrode taps of the battery, with the most obvious performance near the negative electrode taps. Moreover, the battery surface temperature gradually decreases from the position close to the positive and negative electrode tabs to the position away from the positive and negative electrode tabs. The maximum temperature differences between hotspots on the surface of the battery at 0.5C, 1C, and 1.5C rates reach 3.7 °C, 9.4 °C, and 11.3 °C, respectively. Through analysis, it can be found that the temperature difference on the battery surface will increase continuously with the increase in charging and discharging rates.

B. Temperature Field Distribution on the Battery Surface

Figures 4, 5, and 6 correspond to TD maps of the battery surface at different time points under charging and discharging

rates of 0.5C, 1C, and 1.5C, respectively. The TD on the battery charging and discharging can be clearly observed from these temperature maps. Combined with Fig. 3(a-e), the TD on the battery surface during the charging and discharging processes of the 0.5C battery can be analyzed as follows:

i. Figure 4(a) shows the TD on the battery surface in the initial state when the battery has not been charged or discharged yet. Since the battery surface temperature is room temperature at the beginning, the temperature rise on the battery surface is zero.

ii. Figure 4(b) shows the TD on the battery surface at the end of CC discharge. At this time, the voltage drop across the battery has reached its minimum value, and the maximum hotspot on the battery surface is located near the negative electrode taps of the battery, with a temperature rise of 14.9 °C, which is the highest temperature point during the CC discharge surface and the specific location of each hotspot during process. The lowest temperature rise is 11.5 °C, which is located at the lower edge of the battery surface.

iii. Figure 4(c) shows the TD on the battery surface after the battery has been left idle for 30 minutes and the internal state of the battery has stabilized. During the idle period, the chemical reaction and charge distribution inside the battery gradually reach equilibrium, and the internal resistance gradually decreases, which leads to a gradual increase in the voltage across the battery until it reaches a balanced state. During this process, the temperature on the battery surface keeps decreasing. However, as the idle time is only 30 minutes, the temperature on the battery surface has not decreased to room temperature yet, and there is still a temperature rise in the range of 6.0-6.5 °C.

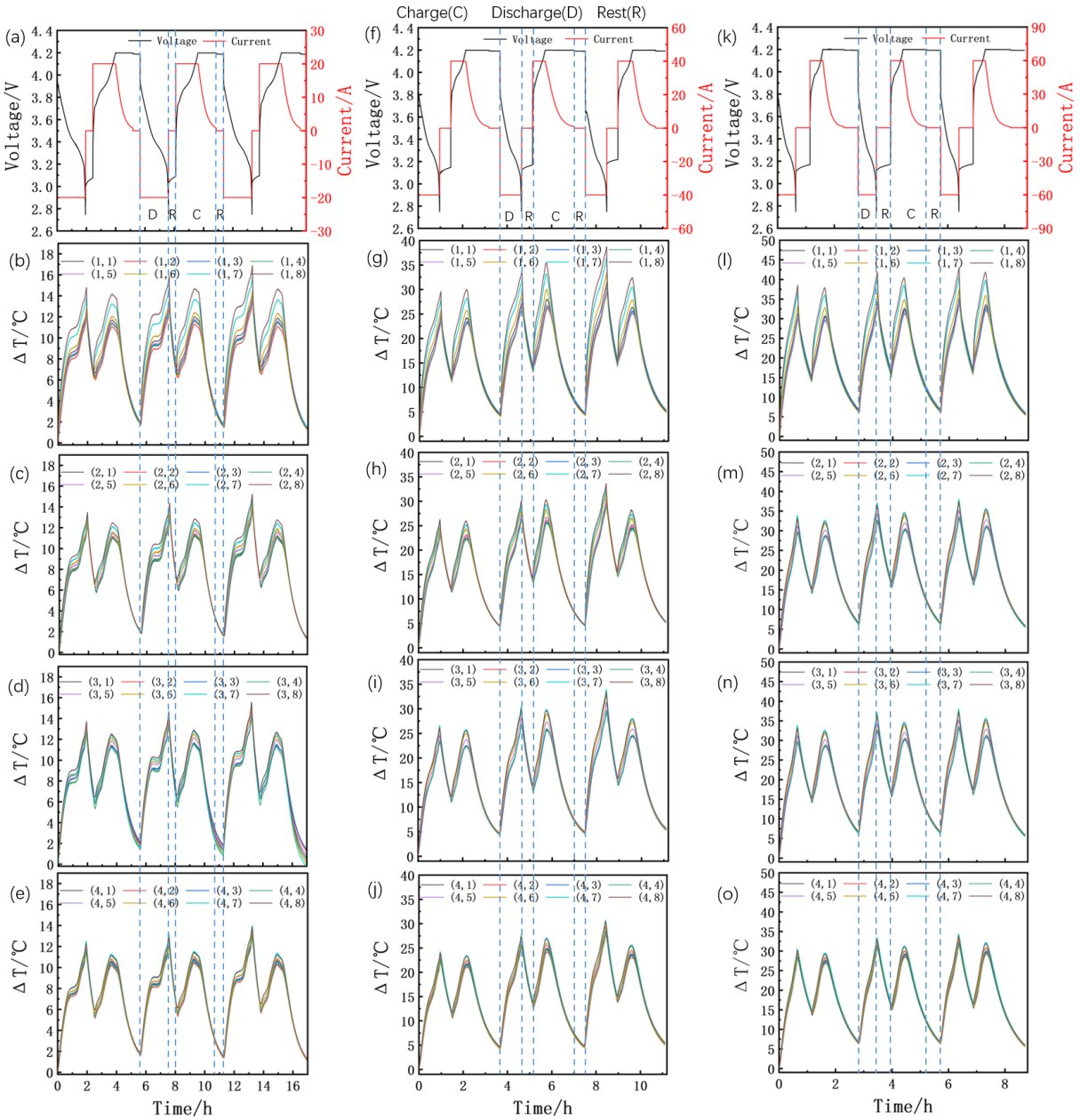

Fig. 3. Voltage, current, and battery surface monitoring point temperature changes at different charging and discharging rates: (a-e) 0.5C, (f-j) 1C, (k-o) 1.5C.

iv. Figure 4(d) shows the TD on the battery surface at the end of CC charging. During the CC charging stage, the voltage across the battery continues to rise to its maximum value of 4.2 V. During this process, the battery surface temperature starts to rise continuously until it reaches its highest point at the end of the CC discharge stage, with a temperature rise in the range of 10.2-14.2 °C.

v. Figure 4(e) shows the TD on the battery surface at the end of CV charging. During this stage, the battery is deeply charged with a CV of 4.2 V. As the charging current decreases continuously, the temperature rise on the battery surface also decreases until it reaches a range of 1.5-2.0 °C at the end of the CV charging.

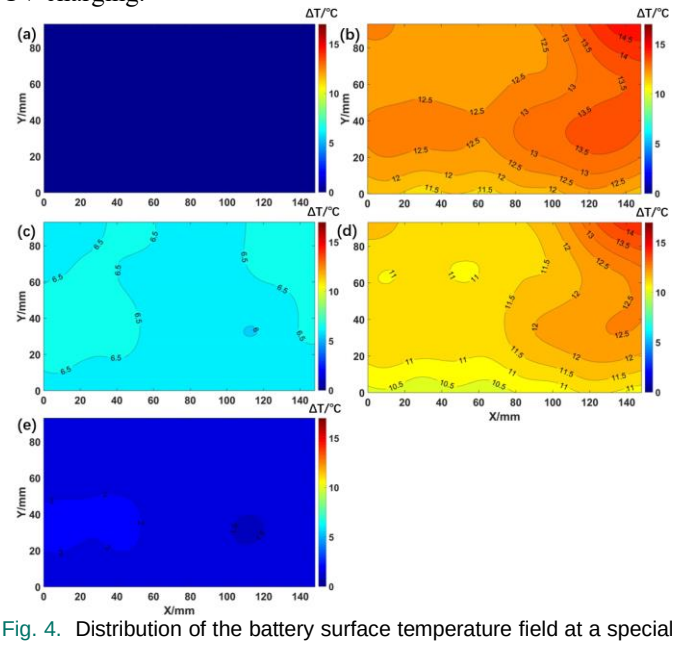

Fig. 4. Distribution of the battery surface temperature field at a special moment in the first cycle of 0.5C: (a) Initial state surface temperature rise; (b) Surface temperature rise after CC discharge; (c) Surface temperature rise after shelving; (d) CC charge surface temperature rise; (e) Surface temperature rise after CV charging.

Comparing the TD of the battery surface at 1C and 1.5C, corresponding to Figs. 5 and 6, with the analysis of the temperature field at 0.5C charging and discharging, it is observed that they exhibit the same trend. At 1C rate, the battery surface temperature increases continuously during constant current charging and discharging, reaching a maximum temperature rise of 29.8 °C and 30.4 °C at the end of discharging and charging, respectively. The maximum temperature difference on the battery surface hotspot also increases to 9.4 °C after CC charging and discharging. At a 1.5C rate, the maximum temperature rises on the battery surface at the two time points mentioned above reach 38.4 °C and 37.8 °C, respectively, and the maximum temperature difference on the battery surface reaches 11.3 °C. In addition, in order to provide a real-time and intuitive reflection of the TD on the battery surface during charging and discharging, we used the temperature rise of 32 temperature points measured by the FBG arrays for linear interpolation operations to construct a dynamic graph of the temperature rise changes on the battery surface. Figures 7, 8, and 9 (attached) show dynamic temperature rise distributions on the battery surface during the first complete charge and discharge cycles at 0.5C, 1C, and 1.5C rates, respectively. In these dynamic figures, the temperature rise distribution on the battery surface is recorded every 10 seconds and displayed at a frame rate of 20 frames per second, providing a clear observation that the temperature at various points on the battery surface rapidly increases during CC charging and discharging. However, the temperature rise rate at each point varies, and as the temperature on the battery surface continues to increase, the temperature difference between hotspots on the battery surface becomes increasingly significant, forming local hotspots.

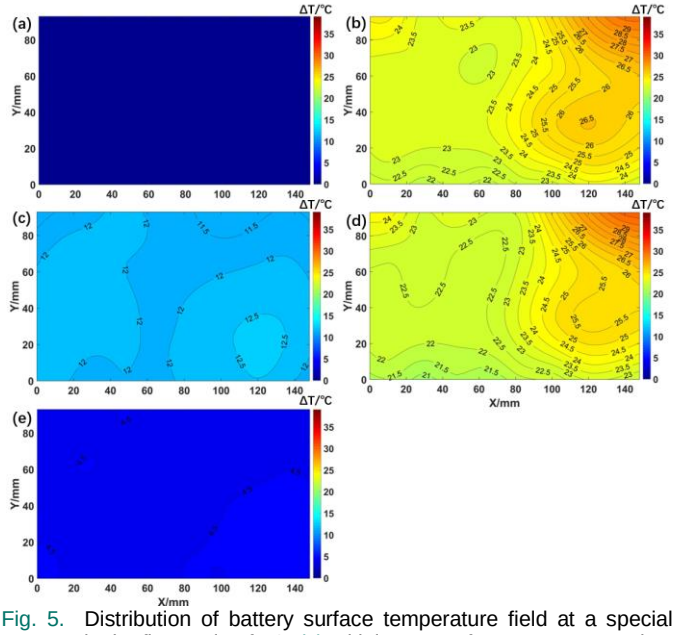

Fig. 5. Distribution of battery surface temperature field at a special moment in the first cycle of 1C: (a) Initial state surface temperature rise; (b) Surface temperature rise after CC discharge; (c) Surface temperature rise after shelving; (d) CC charge surface temperature rise; (e) Surface temperature rise after CV charging.

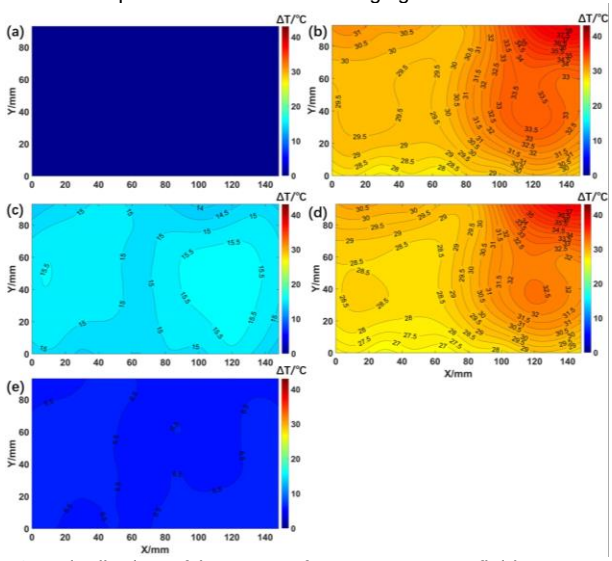

Fig. 6. Distribution of battery surface temperature field at a special moment in the first cycle of 1.5C: (a) Initial state surface temperature rise; (b) Surface temperature rise after CC discharge; (c) Surface temperature rise after shelving; (d) CC charge Surface temperature rise; (e) surface temperature rise after CV charging.

The above research results indicate that the battery surface temperature will increase with the increase of the charging and discharging rate. Moreover, the temperature difference between hotspots on the battery surface will also increase, but the overall TD on the battery surface tends to decrease from the position

close to the positive and negative taps of the battery to the bottom edge of the battery. This may be due to the fact that the main heat generation during battery charging and discharging occurs at the positions of the positive and negative taps of the battery.

IV. Conclusion

In this paper, we present a sensor network consisting of 32 FBG sensors for monitoring the surface TD of a square LiB during charging and discharging cycles, and construct the temperature field on the battery surface based on the measured temperature points. The results show that many hotspots are formed on the battery surface during charging and discharging cycles, and the maximum temperature differences of these hotspots under three charging and discharging rates of 0.5C, 1C, and 1.5C reach 3.7 °C, 9.4 °C, and 11.3 °C, respectively. Moreover, the temperature of the hotspots and the maximum temperature difference between them increase with the increase of the charging and discharging rate. However, the TD on the battery surface always decreases from the positions near the positive and negative electrode tabs to those farther away from the tabs, under the three different charging and discharging rates. The experimental results demonstrate that this sensor is effective in monitoring the temporal and spatial characteristics of hotspots on the battery surface. The proposed FBG sensor network is a promising tool with the advantages of high precision, non-intrusiveness, and low cost, which can improve the thermal management and safety of batteries and accurately identify the key areas where hotspots occur.

References

1. Y. Wang, Q. Gao, G. Wang, P. Lu, M. Zhao, and W. Bao, "A review on research status and key technologies of battery thermal management and its enhanced safety", Int. J. Energ. Res., vol. 42 no. 13, pp. 4008-4033, Oct. 2018.
2. B. Scrosati and J. Garche, "Lithium batteries: Status, prospects and future", J. Power Sources, vol. 195, no. 9, pp. 2419-2430, May. 2010.
3. T. Amietszajew, E. McTurk, J. Fleming, and R. Bhagat, "Understanding the limits of rapid charging using instrumented commercial 18650 high-energy Li-ion cells", Electrochim. Acta, vol. 263, pp. 346-352, Feb. 2018.
4. X. Feng, M. Ouyang, X. Liu, L. Lu, Y. Xia, and X. He, "Thermal runaway mechanism of lithium-ion battery for electric vehicles: A review", Energy Storage Mater., vol. 10, pp. 246-267, Jan. 2018.
5. S. S. Zhang, K. Xu, and T. R. Jow, "Charge and discharge characteristics of a commercial LiCoO2-based 18650 Li-ion battery", J. Power Sources, vol. 160, no. 2, pp. 1403-1409, Oct. 2006.
6. J. Kang and G. Rizzoni, "Study of relationship between temperature and thermal energy, operating conditions as well as environmental factors in large-scale lithium-ion batteries", Int. J. Energ. Res., vol. 38, no. 15, pp. 1994-2002, Dec. 2014.
7. K. M. Alcock, M. Grammel, and Á. González-Vila, "An accessible method of embedding fiber optic sensors on lithium-ion battery surface for in-situ thermal monitoring", Sens. Actuators A, vol. 332, p. 113061, Sep. 2021.
8. B. Li, M. H. Parekh, R. A. Adams, T.E Adams, C.T. Love, V. G. Pol, and V. Tomar, "Lithium-ion battery thermal safety by early internal detection, prediction and prevention", Sci. Rep., vol. 9, no. 1, p. 13255, Sep. 2019.
9. E. Gümüşsu, Ö. Ekici, and M. Köksal, "3-D CFD modeling and experimental testing of thermal behavior of a Li-Ion battery", Appl. Therm. Eng., vol. 120, pp. 484-495, Jun. 2017.
10. J. Huang, L. Albero. Blanquer, J. Bonefacino, and E.R. logan, "Operando decoding of chemical and thermal events in commercial Na (Li)-ion cells via optical sensors", Nat. Energ, vol. 5, no. 9, pp. 674-683, Sep. 2020.
11. C. F. Lopez, J. A. Jeevarajan, and P. P. Mukherjee, "Characterization of lithium-ion battery thermal abuse behavior using experimental and computational analysis", J. Electrochem. Soc., vol. 162, no. 10, p. A2163, Aug. 2015.
12. A. Melcher, C. Ziebert, M. Rohde, and H. J. Seifert, "Modeling and simulation of the thermal runaway behavior of cylindrical Li-ion cells—Computing of critical parameters", Energies, vol. 9, no. 4, p. 292, Apr. 2016.
13. K. Shah, D. Chalise and A. Jain, "Experimental and theoretical analysis of a method to predict thermal runaway in Li-ion cells", J. Power Sources, vol. 330, pp. 167-174, Oct. 2016.
14. M. F. H. Rani, Z. M. Razlan, A. B. Shahriman, and Z. Ibrahim, "Comparative study of surface temperature of lithium-ion polymer cells at different discharging rates by infrared thermography and thermocouple", Int. J. Heat Mass Tran., vol. 153, p. 119595, Jun. 2020.
15. N. Martiny, A. Rheinfeld, J. Geder, Y. Wang, W. Kraus, and A. Jossen, "Development of an all kapton-based thin-film thermocouple matrix for in situ temperature measurement in a lithium-ion pouch cell", IEEE Sens. J., vol. 14, no. 10, pp. 3377-3384, Oct. 2014.
16. S. Goutam, J. M. Timmermans, N. Omar, P. Van. den. Bossche, and J. Van. Mierlo, "Comparative study of surface temperature behavior of commercial li-ion pouch cells of different chemistries and capacities by infrared thermography", Energies, vol. 8, no. 8, pp. 8175-8192, Aug. 2015.
17. A.G. Leal-Junior, A. Frizera, C. Marques, and M. J. Pontes, "Optical fiber specklegram sensors for mechanical measurements: A review", IEEE Sens. J., vol. 20, no. 2, pp. 569-576, Oct. 2019.
18. A. Leal-Junior, A. Theodosiou, C. Díaz, C. Marques, M. J. Pontes, K. Kalli, and A. Frizera-Neto, "Fiber Bragg gratings in CYTOP fibers embedded in a 3D-printed flexible support for assessment of human–robot interaction forces", Materials, vol. 11, no. 11, p. 2305, Nov. 2018.
19. S. Xu, Q. Peng, C. Li, B. Liang, J. Sun, F. Xing, H. Xue, and M. Li, "Optical fiber current sensors based on FBG and magnetostrictive composite materials", Appl. Sci., vol. 11, no. 1, p. 161, Jan. 2021.
20. Z. Wei, J. Hu, H. He, Y. Yu, and J. Marco, "Embedded distributed temperature sensing enabled multistate joint observation of smart lithium-ion battery", IEEE T. Ind. Electron., vol. 70, no. 1, pp. 555-565, Jan. 2023.
21. A. Fortier, M. Tsao, N. D. Williard, Y. Xing, and M. G. Pecht, "Preliminary study on integration of fiber optic Bragg grating sensors in li-ion batteries and in situ strain and temperature monitoring of battery cells", Energies, vol. 10, no. 7, p. 838, Jul. 2017.
22. E. McTurk, T. Amietszajew, J. Fleming, and R. Bhagat, "Thermo-electrochemical instrumentation of cylindrical Li-ion cells", J. Power Sources, vol. 379, pp. 309-316, Mar. 2018.
23. Y. Liu, Z. Liu, W. Mei, X. Han, P. Liu, C. Wang, X. Xia, and K. Li, "Operando monitoring Lithium-ion battery temperature via implanting femtosecond-laser-inscribed optical fiber sensors", Measurement, vol. 203, p. 111961, Nov. 2022.
24. J. Peng, S. Jia, H. Yu, X. Kang, S. Yang, and S. Xu, "Design and experiment of FBG sensors for temperature monitoring on external electrode of lithium-ion batteries", IEEE Sens. J., vol. 21, no. 4, pp. 4628-4634, Feb. 2021.
25. V. Biazi, A. C. Moreira, J. L. Pinto, M. Nascimento, and C. Marques, "A particle filter-based virtual sensor for estimating the state of charge and internal temperature of lithium-ion batteries: Implementation in a simulated study case", J. Energy Storage, vol. 61, p. 106816, May. 2023.
26. L. C. Matuck, P. D. Cabrita, J. L. Pinto, C. A. Marques, and M. S. Nascimento, "Customized Optical Fiber Birefringent Sensors to Multipoint and Simultaneous Temperature and Radial Strain Tracking of Lithium-Ion Batteries", Advanced Sensor Research, vol. 2, no. 7, p. 220046, Feb. 2023.
27. L. Matuck, J. L. Pinto, C. Marques, and M. Nascimento, "Simultaneous Strain and Temperature Discrimination in 18650 Li-ion Batteries Using Polarization-Maintaining Fiber Bragg Gratings", Batteries, vol. 8, no. 11, p. 233, Nov. 2022.
28. J. Peng, S. Jia, H. Yu, X. Kang, S. Yang and S Xu, "Design and experiment of FBG sensors for temperature monitoring on external electrode of lithium-ion batteries", IEEE Sens. J., vol. 21, no. 4, pp.4628-4634, Feb. 2021.

29. M. Nascimento, M. S. Ferreira, and J. L. Pinto, "Real time thermal monitoring of lithium batteries with fiber sensors and thermocouples: A comparative study", Measurement, vol. 111, pp. 260-263, Dec. 2017.
30. M. Nascimento, M. S. Ferreira, and J. L. Pinto, "Temperature fiber sensing of Li-ion batteries under different environmental and operating conditions", Appl. Therm. Eng., vol. 149, pp. 1236-1243, Feb. 2019.
31. M Nascimento, T Paixão, M.S. Ferreira and J.L. Pinto, "Thermal mapping of a lithium polymer batteries pack with FBGs network", Batteries., vol. 4, no. 4, pp. 67, Dec. 2018.
32. J. Sun, G. Wei, L. Pei, R. Lu, K. Song, C. Wu, and C Zhu, "Online internal temperature estimation for lithium-ion batteries based on Kalman filter", Energies, vol. 8, no. 5, pp. 4400-4415, May. 2015.
33. X. Lin, H. E. Perez, J. B. Siegel, A. G. Stefanopoulou, Y. Li, R. D. Anderson, Y. Ding, and M. P. Castanier, "Online parameterization of lumped thermal dynamics in cylindrical lithium-ion batteries for core temperature estimation and health monitoring", IEEE T. Contr. Syst. T., vol. 21, no. 5, pp. 1745-1755, Sep. 2013.
34. C. Forgez, D. V. Do, G. Friedrich, M. Morcrette, and C. Delacourt, "Thermal modeling of a cylindrical LiFePO4/graphite lithium-ion battery", J. Power Sources, vol. 195, no. 9, pp. 2961-2968, May. 2010.
35. K. Hill, B. Malo, F. Bilodeau, D. C. Johnson, and J. Albert, "Bragg gratings fabricated in monomode photosensitive optical fiber by UV exposure through a phase mask", Appl. Phys. Lett., vol. 62, no.10, pp. 1035-1037, May. 1993.

Feixia Huang received the B.S. degree from Nanchang Hangkong University, Nanchang, China, in 2021. He is currently pursuing the M.S. degree in optical engineering with Nanchang Hangkong University, Nanchang, China. His current research interests include optical fiber sensing and structural health monitoring.

Hong Yang received the B.S. and Ph.D. degrees from Nanchang University, China. He is a lecturer with the Key Laboratory of Opto-Electronic Information Science and Technology of Jiangxi Province, Nanchang Hangkong University, China. His current research interests include optical smart metal structure and optical fiber sensing.

Bin Liu (Member, IEEE) received the B.S. and Ph.D. degrees from Sun Yat-sen University, China. Dr. Liu is an Associate Professor with the Key Laboratory of Opto-Electronic Information Science and Technology of Jiangxi Province, Nanchang Hangkong University, China. He has over 80 publications in the area of photonics and holds 10 invention patents. His current research interests include optical fiber interferometer and the application for sensing, fiber bio-chemical sensors, optical micro-cavity and the application for sensing, surface plasmon resonant, Design and application of micro-nano photonic devices, optical nonlinearity and optical soliton, FBG sensing and distributed fiber sensing.

Juan Liu received her Ph.D. degree from Beijing Normal University, China. She is a lecture with Key Laboratory of Nondestructive Test (Ministry of Education) of Nanchang Hangkong University, China. Her main research interest is fiber optic sensing.

Yingying Hu received her Ph.D. degree from University of Science and Technology of China, China. She is a lecture with Key Laboratory of Nondestructive Test (Ministry of Education) of Nanchang Hangkong University, China. Her main research interest is fiber optic sensing and qantum random number.

Yue Fu is a lecturer with the Key Laboratory of Opto-Electronic Information Science and Technology of Jiangxi Province, Nanchang Hangkong University, China. Her current research interests include ultrasonic detection and photoelectric detection.

Wenbo Xiao received the Ph.D. degree in Microelectronics and Solid State Electronics, Institute of Semiconductor, Chinese Academy of Sciences, Beijing, China, in 2008.Dr. Xiao is an Professor with the Key Laboratory of Opto-Electronic Information Science and Technology of Jiangxi Province, Nanchang Hangkong University, China. His research interests include semiconductor device physics and semiconductor photoelectric inspection.

Xing-Dao He was born in Jingan, China, in 1963. He received the Ph.D. degree in optics from Beijing Normal University, Beijing, China, in 2005. He is currently a Professor with the Key Laboratory of Nondestructive Test (Ministry of Education), Nanchang Hangkong University, China. His current research interests include light scattering spectroscopy, optical holography, and information processing.

Qiang Wu received the B.S. and Ph.D. degrees from Beijing Normal University and Beijing University of Posts and Telecommunications, Beijing, China, in 1996 and 2004, respectively. From 2004 to 2006, he worked as a Senior Research Associate in City University of Hong Kong. From 2006 to 2008, he took up a research associate post in Heriot-Watt University, Edinburgh, U.K. From 2008 to 2014, he worked as a Stokes Lecturer at Photonics Research Centre, Dublin Institute of Technology, Ireland. He is an Associate Professor / Reader with Faculty of Engineering and Environment, Northumbria University, Newcastle Upon Tyne, United Kingdom. His research interests include optical fiber interferometers for novel fiber optical couplers and sensors, nanofiber, microsphere sensors for bio-chemical sensing, the design and fabrication of fiber Bragg grating devices and their applications for sensing, nonlinear fiber optics, surface plasmon resonant and surface acoustic wave sensors. He has over 280 publications in the area of photonics and holds 8 invention patents. He is an Editorial Board Member of Scientific Reports, an Associate Editor for IEEE Sensors Journal and an Academic Editor for Journal of Sensors.